



# The Relations between the Various Critical Temperatures of Thin FGM Plates

Ahmed Hassan Ahmed Hassan<sup>1</sup>, Naci Kurgan<sup>2</sup>, Nihat Can<sup>3</sup>

<sup>1</sup> Department of Mechanical Engineering, Ondokuz Mayıs University, Samsun, 55139, Turkey, Email: 15210457@stu.omu.edu.tr

<sup>2</sup> Department of Mechanical Engineering, Ondokuz Mayıs University, Samsun, 55139, Turkey, Email: naci.kurgan@omu.edu.tr

<sup>3</sup> Department of Mechanical Engineering, Ondokuz Mayıs University, Samsun, 55139, Turkey, Email: 13210381@stu.omu.edu.tr

Received August 20 2020; Revised September 07 2020; Accepted for publication September 07 2020.

Corresponding author: A.H.A. Hassan (15210457@stu.omu.edu.tr)

© 2020 Published by Shahid Chamran University of Ahvaz

**Abstract.** This work investigates the relations between the critical temperature of the thin FGM plates under various temperature distributions through the thickness resting on the Pasternak elastic foundation. Both rectangular and skew plates are investigated. The uniform, linear, and nonlinear temperature distributions through the plate's thickness are considered. Formulations are derived based on the classical plate theory (CPT) considering the von Karman geometrical nonlinearity taking the physical neutral plane as the reference plane. The partial differential formulation is separated into two sets of ordinary differential equations using the extended Kantorovich method (EKM). The stability equations and boundary conditions terms are derived according to Trefftz criteria using the variational calculus expressed in an oblique coordinate system. Novel multi-scale plots are presented to show the linear relations between the critical temperatures under various temperature distributions. The critical temperature of plates with different materials are also found linearly related. Resulting relations should be a huge time saver in the analysis process, as by knowing one critical temperature of the one FGM plate under one temperature distribution many other critical temperatures of many other FGM plates under any temperature distributions can be obtained instantly.

**Keywords:** Multi-term extended Kantorovich method; Classical plate theory; Thermal buckling; Functionally graded material; Pasternak elastic foundation.

## 1. Introduction

Back in 1972, an advanced inhomogeneous composite material that has its composition changes gradually between different phases through one or more dimension was theoretically proposed in [1, 2] as an effort to reduce or eliminate the stress concentration that occurs due to the sudden change in the material properties at the interfaces between different phases in the conventional composite materials [3]. That advanced inhomogeneous composite material is called the functionally graded material (FGM). In 1984, the concept of the FGM was implemented in the design of thermal resistant structures [4], as the first engineering application of FGM. Since then, many engineering components have been designed as FGM. Examples of FGM engineering applications and products are presented in [5-10]. When a FGM structure has a wide flat planar surface with relatively small thickness it can be reasonably modeled as a FGM plate. Due to the relative simplicity of the flat plate's structure, many simplified two-dimensional theories were proposed to model the plates. Those plate theories provide accurate enough models while being much simpler to use than the general three-dimensional elasticity theory.

While moderately thick and thick plates have a considerable effect of the transverse shear deformations [11, 12], and the very thin plates as micro- and nano-plates have a considerable scale effect [13-17], thin plates have negligible transverse shear deformations as well as negligible scale effect. This makes thin plates describable with the most simplified plate theory which is the classical plate theory (CPT), developed in 1881 [18]. Many engineering parts and structures are modeled as rectangular or skew plates [19], for example, the tail-fin and swept wings of airplanes [20] are modeled as skew plates. FGM face sheets attached to isotropic core material can be modeled as FGM plates resting on an elastic foundation [21]. The Pasternak model of the elastic foundation is widely used to describe the mechanical interactions between structure and foundation [22]. It treats the bond between the structure and the foundation as two elastic layers, the first has only out-of-plane extension stiffness ( $k_n$ ) and the second has only shear stiffness ( $k_p$ ), as shown in **Fig. 1**. If only the first layer of normal stiffness is considered, the model reduces to the simpler Winkler model.

Mainly, analysis of plates include dynamic [23, 24], and static analyses. The latter analyses include bending [25, 26] and buckling [27, 28] analysis. Selecting an analysis to conduct should be based on the application and conditions for which the plate is designed. In applications where a plate experiences thermal loads, thermal buckling should be one of the conducted analyses in the design process to obtain a correct prediction of the behavior of the plate. Thermal buckling of simply supported rectangular FGM plates not resting on an elastic foundation is solved analytically in [29, 30]. However, for the cases of skew FGM plates as well



as FGM plates resting on elastic foundation, there are only numerical solutions and no analytical ones are found in the literature. The commonly implemented numerical methods in the thermal buckling analysis of FGM plates are the element-free Galerkin's solution (EFG) [31] and the finite element method (FEM) [32, 33]. Another method has gained increasingly interest in the field of computational mechanics is the extended Kantorovich method (EKM). EKM was first proposed by Kerr [34] to solve partial differential equations (PDE) by simplifying the problem to a set of ordinary differential equations (ODE), which are then solved iteratively starting from arbitrary trial functions. Singhatanadgid and Singhanart [35] presented a comprehensive review of the implementation of EKM in the analysis of plates. Just a few studies implemented EKM in the bending analysis of FGM skew plates resting on an elastic foundation. Those studies are [25, 36-39]. However, the only study found in the literature that implemented EKM to the buckling analysis of the skew plates is [27], in which buckling under mechanical loading was considered.

Javaheri and Eslami [29] presented the relation between the critical uniform temperature and the critical rise of linearly changing temperature through the length of the rectangular FGM plate. To the best of the authors' knowledge, the relations between the critical temperatures of FGM plates under various temperature distributions through the thickness have not been investigated yet. In addition, to the best of the authors' knowledge the thermal buckling of skew FGM plates has not been investigated using EKM yet. Implementing EKM to investigate the thermal buckling of skew plates is presented here for the first time. This article aims to use EKM to obtain the numerical solution of the critical temperatures of thin skew plates resting on the Pasternak elastic foundation, and then investigate the relations between those critical temperatures.

Formulations are derived based on the classical plate theory (CPT) considering the von Karman geometrical nonlinearity and taking the physical neutral plane as the reference plane. The stability equations and boundary conditions terms are derived according to Trefftz criteria of the minimum total potential energy using the variational calculus expressed in an oblique coordinate system. This derivation is different in concept than the ones shown in [27, 40-43] in which the stability equations are confused with the equilibrium equations, as they are obtained by equating the first variation of the total potential energy to zero, which is fundamentally wrong, as explained in [44]. This article illustrates in detail the correct derivation of the stability equations and the boundary conditions of the plates resting on elastic foundation using EKM.

The previously published works on this topic, e.g., the recent book [45], investigate each of the critical temperatures individually. In other words, they intend to find the analytical or numerical solutions of the critical temperature of the FGM plate under each different temperature distribution separately. In this article, in addition to the derivation of the numerical solution method using EKM, further investigation of the linear relations between the critical temperatures is also presented. The relations between the critical temperatures of plates with different materials are also investigated. Resulting relations should be a huge time saver in the analysis process, as by knowing one critical temperature of the one FGM plate under one temperature distribution many other critical temperatures of many other FGM plates under any temperature distribution through the thickness can be obtained instantly.

The article starts with the derivation of the separated stability equations and boundary conditions, and then the validation of the method by comparing the results with those found in the literature. Lastly, the linear relations between the critical temperatures are derived and discussed.

### 2. Oblique Coordinate System and Transformations

Considering the coordinate systems presented in Fig. 2, the transformation between the oblique ( $\xi - \eta$ ) and the Cartesian ( $x - y$ ) coordinate systems is governed by the skew angle  $\phi$  as

$$\begin{bmatrix} x \\ y \end{bmatrix} = \begin{bmatrix} 1 & s \\ 0 & c \end{bmatrix} \begin{bmatrix} \xi \\ \eta \end{bmatrix} \quad c = \cos \phi \quad s = \sin \phi \tag{1}$$

As shown in [25, 27] the functions in the ( $x - y$ ) coordinates can be transformed into the corresponding functions in the ( $\xi - \eta$ ) coordinate system by using eq. (1). The considered oblique coordinate system is the one having each axis parallel to two opposite edges of the plate.

### 3. Stability Equations and Boundary Conditions

The stability equation and boundary conditions are derived here based on the minimum potential energy criterion, also known as Trefftz criterion [44], expressed as

$$\delta(\bar{\delta}^2 e_p) = 0 \tag{2}$$

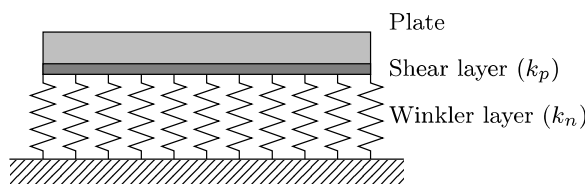


Fig. 1. Schematic of FGM plate resting on the Pasternak elastic foundation

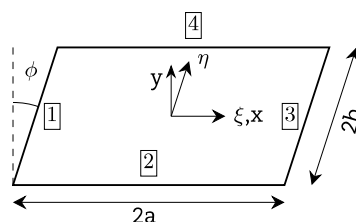


Fig. 2. Coordinate systems convention and edge labeling



where  $\delta^2 e_p$  is the second variation of the potential energy evaluated at the equilibrium state prior to the buckling, i.e.  $(\delta e_p = 0)$ . The total potential energy  $e_p$  of a plate resting on the Pasternak elastic foundation is the summation of the potential energy of the plate  $U_p$  and the potential energy of the elastic foundation  $F_p$ .

$$e_p = U_p + F_p \tag{3}$$

$U_p$  of a thin rectangular plate having dimension  $2a \times 2b$  and thickness  $h$ , is given as

$$U_p = \frac{1}{2} \int_{-a}^a \int_{-b}^b \int_{-h/2}^{h/2} [\sigma_{xx} \bar{\epsilon}_{xx} + \sigma_{yy} \bar{\epsilon}_{yy} + \sigma_{zz} \bar{\epsilon}_{zz} + 2\bar{\gamma}_{xy} \tau_{xy} + 2\bar{\gamma}_{xz} \tau_{xz} + 2\bar{\gamma}_{yz} \tau_{yz}] dz dx dy \tag{4}$$

where  $\bar{\epsilon}_{xx}$ ,  $\bar{\epsilon}_{yy}$ , and  $\bar{\epsilon}_{zz}$  are the normal strains, and  $\bar{\gamma}_{xy}$ ,  $\bar{\gamma}_{yz}$ , and  $\bar{\gamma}_{xz}$  are the shear strains in the stated directions. Normal stress components are  $\sigma_{xx}$ ,  $\sigma_{yy}$ , and  $\sigma_{zz}$ , and the shear stress components are  $\tau_{xy}$ ,  $\tau_{yz}$ , and  $\tau_{xz}$  in the stated directions. To find those stress and strain components for a thin plate, the classical plate theory (CPT) is adopted. CPT states the following constitutive equations.

$$\bar{w} = w \quad \bar{u} = u - (z - z_0)w_{,x} \quad \bar{v} = v - (z - z_0)w_{,y} \tag{5}$$

where  $\bar{u}$ ,  $\bar{v}$ , and  $\bar{w}$  are the displacements of any point of the plate in the directions  $x$ ,  $y$ , and  $z$ , respectively.  $z_0$  is the offset between the midplane and the physical neutral plane through the thickness of the plate.  $u$ ,  $v$ , and  $w$  are the displacements of any point at the physical neutral plane. The physical neutral plane is the plane at which the resultant of the bending moment  $B_0$  vanishes [46]. The distance between the midplane ( $z = 0$ ) and the physical neutral plane ( $z = z_0$ ) is obtained from the following equation [46].

$$B_0 = \int_{-h/2}^{h/2} [(z - z_0)E_{(z)}] dz = 0 \tag{6}$$

where  $E_{(z)}$  is Young's elasticity modulus as a function of  $z$ . Note that if  $E_{(z)}$  is constant or symmetric about the midplane then  $z_0$  vanishes and the physical neutral plane will coincide with the midplane. The cross-section of a typical FGM plate is shown in Fig. 3.

Considering the von Karman nonlinearities, strains are related to the displacements by the following equations.

$$\begin{aligned} \bar{\epsilon}_{xx} &= \bar{u}_{,x} + \frac{1}{2}(\bar{w}_{,x})^2 & \bar{\gamma}_{xy} &= \frac{1}{2}(\bar{u}_{,y} + \bar{v}_{,x} + \bar{w}_{,x}\bar{w}_{,y}) \\ \bar{\epsilon}_{yy} &= \bar{v}_{,y} + \frac{1}{2}(\bar{w}_{,y})^2 & \gamma_{xz} &= \gamma_{yz} = \epsilon_{zz} = 0 \end{aligned} \tag{7}$$

The subscripts after commas denote the partial derivatives in the stated directions. Stresses are related to the strains as follows.

$$\begin{aligned} \sigma_{xx} &= \frac{E_{(z)}}{1 - \mu^2} ((\bar{\epsilon}_{xx} - \alpha_{(z)} \Delta T_{(z)}) + \mu(\bar{\epsilon}_{yy} - \alpha_{(z)} \Delta T_{(z)})) & \tau_{xy} &= \frac{E_{(z)}}{2(1 + \mu)} \bar{\gamma}_{xy} \\ \sigma_{yy} &= \frac{E_{(z)}}{1 - \mu^2} ((\bar{\epsilon}_{yy} - \alpha_{(z)} \Delta T_{(z)}) + \mu(\bar{\epsilon}_{xx} - \alpha_{(z)} \Delta T_{(z)})) & \tau_{xz} &= \tau_{yz} = \sigma_{zz} = 0 \end{aligned} \tag{8}$$

where  $\mu$  is the Poisson's ratio.  $\alpha_{(z)}$  is the coefficient of thermal expansion.  $\Delta T_{(z)}$  is the temperature increment from a reference state  $T_0$ , i.e.

$$\Delta T_{(z)} = T_{(z)} - T_0 \tag{9}$$

The thermal load will produce stresses in the plate only if is partially or fully restrained from expansion/retraction. Equation (9) expresses the case of full restriction of thermal expansion/retraction of the plate. Lastly, the second component of  $e_p$  of eq. (3) is the potential energy of the Pasternak elastic foundation  $F_p$ , which consists of normal and shear stiffness ( $k_n$ ,  $k_p$ ), and given as

$$F_p = \frac{1}{2} \int_{-b}^b \int_{-a}^a [k_n w^2 + k_p ((w_{,x})^2 + (w_{,y})^2)] dx dy \tag{10}$$

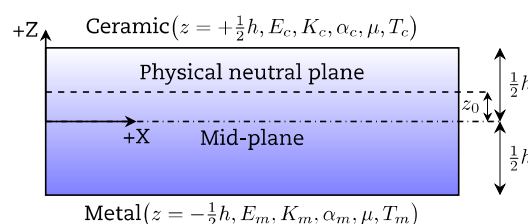


**Fig. 3.** Cross-section of a typical FGM plate having its material composition varying from ceramic at the top surface to metal at its bottom surface, and its physical neutral plane is at offset distance  $z_0$  from the mid-plane



Substituting the constitutive equations of eq. (5) in eq. (7) and then in eq. (8) reveals the stress and strain components in terms of  $u, v,$  and  $w$  and their derivatives. Substituting those stresses and strains in eq. (4) gives  $U_p$ , which is then added to  $F_p$  of eq. (10) to give  $e_p$  of eq. (3) as a functional of  $u_{(x,y)}, v_{(x,y)}$  and  $w_{(x,y)}$ .

$$e_{p(u,v,w)} = \frac{1}{8} \int_{-b}^b \int_{-a}^a \left[ \begin{aligned} &4k_n w^2 + 4k_p \left( (w_{,y})^2 + (w_{,x})^2 \right) + 4D \left( (w_{,yy})^2 + 2(1-\mu)(w_{,xy})^2 + (w_{,xx})^2 + 2\mu w_{,xx} w_{,yy} \right) \\ &+ A \left( \begin{aligned} &2(1-\mu)(u_y + v_x)^2 + 4(u_x^2 + v_y^2) + 8\mu v_y u_x + \left( (w_{,x})^2 + (w_{,y})^2 \right)^2 \\ &+ 4 \left( (w_{,x})^2 (\mu v_y + u_x) + (w_{,y})^2 (v_y + \mu u_x) + w_y w_x (1-\mu)(u_y + v_x) \right) \end{aligned} \right) \\ &- 4\theta(1+\mu) \left( u_x + (w_{,x})^2 + v_y + (w_{,y})^2 \right) + 4\hat{\theta}(1+\mu)(w_{,yy} + w_{,xx}) \\ &- 8B_0 \left( \begin{aligned} &w_{,yy} (v_y + \mu u_x + \mu (w_{,x})^2 + (w_{,y})^2) + (1-\mu) w_{,xy} (u_y + v_x + w_{,y} w_x) \\ &+ w_{,xx} (\mu v_y + u_x + (w_{,x})^2 + \mu (w_{,y})^2) \end{aligned} \right) \end{aligned} \right] dx dy \tag{11}$$

where  $D$  and  $A$  are integrals known as the bending and extension stiffness, respectively.  $\theta$  and  $\hat{\theta}$  are integrals contain  $\Delta T_{(z)}$ . Those integrals are given as follows.

$$\begin{aligned} D &= \int_{-h/2}^{h/2} \left[ \frac{(z-z_0)^2 E_{(z)}}{1-\mu^2} \right] dz & A &= \int_{-h/2}^{h/2} \left[ \frac{E_{(z)}}{1-\mu^2} \right] dz \\ \theta &= \int_{-h/2}^{h/2} \left[ \frac{E_{(z)} \alpha_{(z)} \Delta T_{(z)}}{1-\mu^2} \right] dz & \hat{\theta} &= \int_{-h/2}^{h/2} \left[ \frac{(z-z_0) E_{(z)} \alpha_{(z)} \Delta T_{(z)}}{1-\mu^2} \right] dz \end{aligned} \tag{12}$$

Note that the last group of terms in eq. (11) will vanish as they are all multiplied by  $B_0$ , which is zero by definition as shown in eq. (6).  $\delta^2 e_p$ , the second variation of the total potential energy, is obtained as follows.

$$\delta^2 e = \frac{1}{2} \int_{-b}^b \int_{-a}^a \left[ \begin{aligned} &2k_n (\delta w)^2 + 2k_p \left( (\delta w_{,y})^2 + (\delta w_{,x})^2 \right) + 2D \left( 2\mu \delta w_{,xx} \delta w_{,yy} + 2(1-\mu)(\delta w_{,xy})^2 + (\delta w_{,yy})^2 + (\delta w_{,xx})^2 \right) \\ &+ (\delta w_{,x})^2 \left( A \left( 2(u_x + \mu v_y) + (w_{,y})^2 + 3(w_{,x})^2 \right) - 2\theta(1+\mu) \right) + (\delta w_{,y})^2 \left( A \left( 2(\mu u_x + v_y) + 3(w_{,y})^2 + (w_{,x})^2 \right) - 2\theta(1+\mu) \right) \\ &+ \delta w_{,y} \delta w_{,x} A \left( 2(1-\mu)(u_y + v_x) + 4w_{,y} w_x \right) + \delta w_{,y} A \left( 2w_x (1-\mu)(\delta u_y + \delta v_x) + 4w_{,y} (\mu \delta u_x + \delta v_y) \right) + 2A (\delta v_y)^2 \\ &+ (1-\mu) A (\delta u_y + \delta v_x)^2 + 4A \mu \delta u_x \delta v_y + \delta w_{,x} A \left( 2w_y (1-\mu)(\delta u_y + \delta v_x) + 4w_{,x} (\delta u_x + \mu \delta v_y) \right) + 4A \mu \delta u_x \delta v_y \end{aligned} \right] dx dy \tag{13}$$

where  $\delta u, \delta v, \delta w, \delta u_x, \delta u_y, \delta v_x, \delta v_y, \delta w_x, \delta w_y, \delta w_{,xx}, \delta w_{,yy}$ , and  $\delta w_{,xy}$  are the variational displacements and their derivatives. The equilibrium of the flat plate implies that no lateral displacement occurs before the buckling point. Therefore, the lateral displacement  $w$  terms and its derivatives in  $\delta^2 e_p$  of eq. (13) vanish. Eliminating the  $w$  terms from  $\delta^2 e_p$  gives  $\bar{\delta}^2 e_p$ . Furthermore, note that after eliminating  $w$  and its derivatives the remaining terms multiplied by  $(\delta w_{,x})^2, (\delta w_{,y})^2$  and  $\delta w_y \delta w_x$  contain nothing but the integrals of the equilibrium state stress component  $\sigma_{xx}, \sigma_{yy}$  and  $\tau_{xy}$ , respectively. Those integrals are called the resultant forces  $N_{xx}, N_{yy}$ , and  $N_{xy}$ , and given eq. (14) by integrating the stress components of eq. (8) with minor rearrangement using the notation shown in eq. (12).

$$\begin{bmatrix} N_{xx} \\ N_{yy} \\ N_{xy} \end{bmatrix} = \int_{-h/2}^{h/2} \begin{bmatrix} \sigma_{xx} \\ \sigma_{yy} \\ \tau_{xy} \end{bmatrix} dz = \begin{bmatrix} A(u_x + \mu v_y) - \theta(1+\mu) \\ A(\mu u_x + v_y) - \theta(1+\mu) \\ \frac{A}{2}(1-\mu)(u_y + v_x) \end{bmatrix} = \begin{bmatrix} -N_T \\ -N_T \\ 0 \end{bmatrix} \tag{14}$$

where  $N_T$  is the resultant force from the thermal load. From eq. (13) with  $w$  and its derivatives being eliminated, eq. (14),  $\bar{\delta}^2 e_p$  can be written as follows.

$$\begin{aligned} \bar{\delta}^2 e_{p(u,v,w,\delta u,\delta v,\delta w)} &= \bar{\delta}^2 \widehat{e}_p + \bar{\delta}^2 \widetilde{e}_p \\ \bar{\delta}^2 \widehat{e}_p &= \int_{-b}^b \int_{-a}^a \left[ \begin{aligned} &k_n (\delta w)^2 + k_p \left( (\delta w_{,y})^2 + (\delta w_{,x})^2 \right) + D \left( 2\mu \delta w_{,xx} \delta w_{,yy} + 2(1-\mu)(\delta w_{,xy})^2 + (\delta w_{,yy})^2 + (\delta w_{,xx})^2 \right) \\ &+ N_{xx} (\delta w_{,x})^2 + N_{yy} (\delta w_{,y})^2 + 2N_{xy} \delta w_y \delta w_x \end{aligned} \right] dx dy \\ \bar{\delta}^2 \widetilde{e}_p &= \frac{A}{2} \int_{-b}^b \int_{-a}^a \left[ (1-\mu)(\delta u_y + \delta v_x)^2 + 2(\delta u_x)^2 + 2(\delta v_y)^2 + 4\mu \delta u_x \delta v_y \right] dx dy \end{aligned} \tag{15}$$

In eq. (15),  $\bar{\delta}^2 e_p$  is written as a summation of two uncoupled integrals. The first integral,  $\bar{\delta}^2 \widehat{e}_p$ , is a functional of  $\delta w$  only and contains neither  $\delta u$  nor  $\delta v$  terms, while the second integral,  $\bar{\delta}^2 \widetilde{e}_p$ , is a functional of  $\delta u$  and  $\delta v$  only, and has no  $\delta w$  terms. Therefore, a further variation of  $\bar{\delta}^2 e_p$  results in an uncoupled set of equations. In addition,  $\bar{\delta}^2 \widehat{e}_p$  contains the resultant force components, while the  $\bar{\delta}^2 \widetilde{e}_p$  doesn't. So, it is safe to drop  $\bar{\delta}^2 \widetilde{e}_p$  and only consider  $\bar{\delta}^2 \widehat{e}_p$  while being sure that will not affect the resulting set of stability equations.



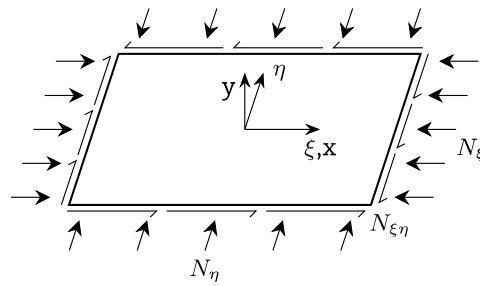


**Fig. 4.** Components of the resultant in-plane forces in the oblique coordinates ( $\xi - \eta$ )

The next step is to transform all the terms of  $\bar{\delta}^2 \widehat{e}_p$  into the oblique coordinates using the transformation function shown in Section 2. Note that the resultant forces  $N_{xx}$ ,  $N_{yy}$ , and  $N_{xy}$  are transformed to the oblique coordinates as illustrated by Wang and Yuan [47] and shown in eq. (16).

$$N_x = \frac{1}{c}(N_\xi + 2sN_{\xi\eta} + s^2 N_\eta) \quad N_y = cN_\eta \quad N_{xy} = N_{\xi\eta} + sN_\eta \tag{16}$$

where  $N_\xi$  and  $N_\eta$  are resultant the normal forces, and  $N_{\xi\eta}$  is the resultants shear force in the oblique coordinates, as shown in **Fig. 4**.

Then, solving eq. (16) for  $N_\xi$ ,  $N_\eta$  and  $N_{\xi\eta}$  in terms of the resultant thermal force  $N_T$  that defined in eq. (14), gives the following.

$$N_\xi = \frac{-N_T}{c} \quad N_\eta = \frac{-N_T}{c} \quad N_{\xi\eta} = \frac{sN_T}{c} \tag{17}$$

Substituting eq. (17) and eq. (16) in eq. (15) and then implementing the coordinates transformation as presented in [27] gives  $\bar{\delta}^2 \widehat{e}_p$  as functional of the function  $\delta w_{(\xi,\eta)}$ , as

$$\bar{\delta}^2 \widehat{e}_p = \int_{-b}^b \int_{-a}^a \left[ \begin{aligned} &k_n (\delta w)^2 + \frac{k_p}{c} ((\delta w_{,\xi})^2 + (\delta w_{,\eta})^2 - 2s\delta w_{,\xi} \delta w_{,\eta}) \\ &+ \frac{D}{c^3} ((\delta w_{,\xi\xi})^2 + (\delta w_{,\eta\eta})^2 + 2R_1 \delta w_{,\xi\xi} \delta w_{,\eta\eta} - 4s\delta w_{,\xi\eta} (\delta w_{,\xi\xi} + \delta w_{,\eta\eta}) + 2R_2 (\delta w_{,\xi\eta})^2) \\ &- \frac{N_T}{c} (\delta w_{,\xi})^2 - \frac{N_T}{c} (\delta w_{,\eta})^2 + 2 \frac{sN_T}{c} \delta w_{,\xi} \delta w_{,\eta} \end{aligned} \right] d\xi d\eta \tag{18}$$

where  $R_1$  and  $R_2$  are constants given as  $R_1 = s^2 + \mu c^2$  and  $R_2 = R_1 - 1$ . The next step is to implement the EKM concept of expressing the unknown bivariate function  $\delta w_{(\xi,\eta)}$  as the summation of  $t$  terms, each is a multiplication of univariate functions of different variables, as illustrated [25, 27].

$$\delta w_{(\xi,\eta)} = f_{(\xi)} g_{(\eta)} = f g \tag{19}$$

The functional  $\bar{\delta}^2 \widehat{e}_p$  becomes as follows.

$$\bar{\delta}^2 \widehat{e}_{p(f,g)} = \int_{-b}^b \int_{-a}^a \left[ \begin{aligned} &k_n (f g)^2 + \frac{k_p}{c} ((f' g)^2 + (f g')^2 - 2s(f' g)(f g')) \\ &+ \frac{D}{c^3} ((f'' g)^2 + (f g'')^2 + 2R_1 (f'' g)(f g'') - 4s(f' g')(f'' g + f g'') + 2R_2 (f' g')^2) \\ &- \frac{N_T}{c} (f' g)^2 - \frac{N_T}{c} (f g')^2 + 2 \frac{sN_T}{c} (f' g)(f g') \end{aligned} \right] d\xi d\eta + \tag{20}$$

From the definition of the temperature increment in eq. (9) along with eq. (14) and eq. (12),  $N_T$  can be expressed as

$$N_T = (1 + \mu)\theta = (1 + \mu) \int_{-h/2}^{h/2} \left[ \frac{E_{(z)} \alpha_{(z)} \Delta T_{(z)}}{1 - \mu^2} \right] dz = \int_{-h/2}^{h/2} \left[ \frac{E_{(z)} \alpha_{(z)} (T_{(z)} - T_0)}{1 - \mu} \right] dz = G_1 - G_2 \tag{21}$$

where  $G_1$  and  $G_2$  are the integrals given as follows.

$$G_1 = \int_{-h/2}^{h/2} [\hat{\mu} E_{(z)} \alpha_{(z)} T_{(z)}] dz \quad G_2 = \int_{-h/2}^{h/2} [\hat{\mu} E_{(z)} \alpha_{(z)} T_0] dz \quad \hat{\mu} = \frac{1}{1 - \mu} \tag{22}$$

Assuming the functions  $f$  are all known, then the two-dimensional functional  $\bar{\delta}^2 \widehat{e}_{p(f,g)}$  in eq. (20) is reduced to a one-dimensional functional of the functions  $g$ . The stability  $\bar{\delta}^2 \widehat{e}_p$  equations are now obtainable by substituting  $\bar{\delta}^2 \widehat{e}_{p(f,g)}$  in the Trefftz criteria shown in eq. (23):



$$\begin{aligned} \delta(\bar{\delta}^2 \widehat{e}_{p(g)}) &= 0 \\ &= 2 \int_{-b}^b \delta_g \left[ \frac{D}{c^3} (R_1 A_{(2,0)} g'' + A_{(2,2)} g - 2sA_{(2,1)} g') + k_n c A_{(0,0)} g + \frac{k_p}{c} (A_{(1,1)} g - sA_{(1,0)} g') - \frac{1}{c} (G_1 - G_2) A_{(1,1)} g + \frac{s}{c} (G_1 - G_2) A_{(1,0)} g' \right] d\eta \\ &\quad + 2 \int_{-b}^b \delta_g' \left[ \frac{D}{c^3} (-2R_2 A_{(1,1)} g' - 2sA_{(1,0)} g'' - 2sA_{(1,2)} g) + \frac{k_p}{c} (A_{(0,0)} g' - sA_{(0,1)} g) - \frac{1}{c} (G_1 - G_2) A_{(0,0)} g' + \frac{s}{c} (G_1 - G_2) A_{(0,1)} g \right] d\eta \\ &\quad + 2 \int_{-b}^b \delta_g'' \left[ \frac{D}{c^3} (A_{(0,0)} g'' - 2sA_{(0,1)} g' + R_1 A_{(0,2)} g) \right] d\eta \end{aligned} \tag{23}$$

where  $A_{(i,j)}$  are  $(t \times t)$  matrices, given by

$$A_{(i,j)} = \int_{-a}^a \left[ \frac{d^i f}{d\xi^i} \right]^T \left[ \frac{d^j f}{d\xi^j} \right] d\xi \tag{24}$$

Implementing the integration by parts on each integral contains derivatives of  $\delta_g$  gives

$$\delta(\bar{\delta}^2 \widehat{e}_{p(g)}) = 0 = \int_{-b}^b \delta_g [H_1 + H_{T01} + H_{T1}] d\eta + \delta_g [H_2 + H_{T02} + H_{T2}]_{-b}^{+b} + \delta_g' [H_3]_{-b}^{+b} \tag{25}$$

where  $H$ 's are single-column matrices  $(t \times 1)$ , obtained as

$$\begin{aligned} H_1 &= \frac{D}{c^3} [A_{(0,0)} g'''' + 2sQ_{(1,0)} g''' - 2sQ_{(2,1)} g' + A_{(2,2)} g + (2R_2 A_{(1,1)} + R_1 (A_{(2,0)} + A_{(0,2)})) g''] + k_n [cA_{(0,0)} g] + \frac{k_p}{c} [A_{(1,1)} g - sQ_{(1,0)} g' - A_{(0,0)} g''] \\ H_2 &= \frac{D}{c^3} [-A_{(0,0)} g''' - 2sQ_{(1,0)} g'' - (2R_2 A_{(1,1)} + R_1 A_{(0,2)}) g' - 2sA_{(1,2)} g] + \frac{k_p}{c} [A_{(0,0)} g' - sA_{(0,1)} g] \\ H_3 &= \frac{D}{c^3} [A_{(0,0)} g'' - 2sA_{(0,1)} g' + R_1 A_{(0,2)} g] \\ H_{T01} &= \frac{G_2}{c} [-A_{(0,0)} g'' - sQ_{(1,0)} g' + A_{(1,1)} g] \\ H_{T02} &= \frac{G_2}{c} [A_{(0,0)} g' - sA_{(0,1)} g] \\ H_{T1} &= \frac{G_1}{c} [A_{(0,0)} g'' + sQ_{(1,0)} g' - A_{(1,1)} g] \\ H_{T2} &= \frac{G_1}{c} [-A_{(0,0)} g' + sA_{(0,1)} g] \end{aligned} \tag{26}$$

where  $Q_{(i,j)}$  are  $(t \times t)$  matrices, given by

$$Q_{(i,j)} = A_{(i,j)} - A_{(j,i)} \tag{27}$$

Since  $\bar{\delta}_g$  is an arbitrary function, each of the three summed parts in eq. (25) has to vanish. Equating the integral part to zero produces  $t$  linear ordinary differential equations (ODE) that have to be satisfied through the interval  $(-b, +b)$ , i.e. the governing system of equations. In order to obtain a nontrivial solution, the following governing equations have to be satisfied.

$$H_1 + H_{T1} + H_{T01} = 0 \tag{28}$$

Equating each of the latter two parts to zero produces two systems of equations, each has  $t$  linear ODE's that have to be satisfied at the boundary points  $(-b$  and  $+b)$ , i.e. the boundary conditions, given as

$$\begin{aligned} \text{either } & g = 0 & \text{or } & H_2 + H_{T02} + H_{T2} = 0 \\ \text{and either } & g' = 0 & \text{or } & H_3 = 0 \end{aligned} \tag{29}$$

To find the buckling factor  $\lambda$  of the thermal loads, the governing equations in eq. (28) are rewritten as a generalized eigenvalue problem as follows.

$$H_1 + H_{T01} = -\lambda H_{T1} \tag{30}$$

with the boundary conditions rewritten as

$$\begin{aligned} \text{either } & g = 0 & \text{or } & H_2 + H_{T02} + \lambda H_{T2} = 0 \\ \text{and either } & g' = 0 & \text{or } & H_3 = 0 \end{aligned} \tag{31}$$

Solving this generalized eigenvalue problem gives the buckling factor  $\lambda$  as the first eigenvalue, and a set of  $t$  functions represents  $g$ . Each edge of the plate can be either clamped (C) having  $(g = g' = 0)$ , simply supported (S) having  $(g = H_3 = 0)$ , or free (F) having  $(H_2 + H_{T02} + \lambda H_{T2} = H_3 = 0)$ . The boundary conditions of a plate are described by stating the boundary condition of each edge in the counterclockwise direction, starting from the left edge, as shown in **Fig. 2**, in which the labeling sequence is written beside the edges. For example, (CSFC) means that edge:  $(\xi = -a)$  is clamped, edge:  $(\eta = -b)$  is simply supported, edge:  $(\xi = +a)$  is free and edge:  $(\eta = +b)$  is clamped.



**Table 1.** Material properties of the constituents of the Al/Al<sub>2</sub>O<sub>3</sub> FGM

Material	E (GPa)	μ	α (/ °C)	K (W /m °C)
Aluminum (Al)	70	0.3	23.0 ×10 <sup>-6</sup>	204.0
Alumina (Al <sub>2</sub> O <sub>3</sub> )	380	0.3	7.4 ×10 <sup>-6</sup>	10.4

### 4. FGM Properties

The classical functionally graded material (FGM) used in the published studies on the plate’s thermal buckling is the aluminum/alumina (Al/Al<sub>2</sub>O<sub>3</sub>) FGM, as it is one of the common materials used to make thermal barriers [48]. The properties of its constituents are shown in Table 1. As assumed in the derivation of the stability equations, the properties of the plate vary in the thickness direction. The variation function is normally the simple power-law, as in [25, 26], but it can also be exponential as in [28], or any other continuous single function. It may be also modeled as a discrete function for the case of sandwich plate as in [24].

A comprehensive review of the variation functions of the FGM plates considered in the thermo-mechanical buckling analysis is provided in [3]. The variation of properties used in this study is the simple power law. This variation of effective properties can be obtained by making the constituents of the FGM change by the desired function and assume that properties at any point are derived using the Voigt’s model. The effective properties are then given as follows.

$$\begin{aligned}
 E_{(z)} &= E_m + E_{cm} V_{(z)}^n & \alpha_{(z)} &= \alpha_m + \alpha_{cm} V_{(z)}^n & K_{(z)} &= K_m + K_{cm} V_{(z)}^n \\
 E_{cm} &= E_c - E_m & \alpha_{cm} &= \alpha_c - \alpha_m & K_{cm} &= K_c - K_m \\
 \mu_{(z)} &= \mu_m = \mu_c & V_{(z)} &= \frac{2z + h}{2h}
 \end{aligned}
 \tag{32}$$

where the subscripts *m* and *c* are used to indicate the properties of the metallic constituent (Al) and the ceramic constituent (Al<sub>2</sub>O<sub>3</sub>), respectively, as shown in Fig. 3. *n* is the gradient index. *V*<sub>(*z*)</sub> is the ceramic volume fraction. *K<sub>c</sub>* and *K<sub>m</sub>* are the conductivity coefficients of the ceramic and metallic constituents, respectively. Note that, if (*n* = 0), then the plate becomes pure ceramic, else, if (*n* = ∞) the plate becomes pure metallic, otherwise, the plate is an FGM consisting of both the ceramic and metallic material. In the latter case, the material composition varies continuously through the thickness according to the given function from pure metallic at the bottom of the plate to pure ceramic at the top.

### 5. Temperature Distribution

The temperature distribution *T*<sub>(*z*)</sub> through the thickness is either uniform, linear, or nonlinear. The uniform and linear distributions of temperature are given by simple formulae as following.

$$\begin{aligned}
 \text{Uniform :} & & T_{(z)} &= T_m = T_c \\
 \text{Linear :} & & T_{(z)} &= T_m + (T_c - T_m) \left( \frac{2z + h}{2h} \right)
 \end{aligned}
 \tag{33}$$

The nonlinear distribution is obtained by solving the heat conduction problem [49] shown in eq. (34).

$$\frac{-d}{dz} \left( K_{(z)} \frac{dT}{dz} \right) = 0
 \tag{34}$$

The solution of this ordinary differential equation is the nonlinear distribution of temperature given as follows [32, 50].

$$\text{Nonlinear :} \quad T_{(z)} = T_m + (T_c - T_m) \int_{-h/2}^z \left[ \frac{1}{K_{(z)}} \right] dz \bigg/ \int_{-h/2}^{h/2} \left[ \frac{1}{K_{(z)}} \right] dz
 \tag{35}$$

Conventionally, the thermal buckling problem is to find the critical uniform temperature Δ*T*<sub>U</sub><sup>cr</sup> in the case of the uniform temperature rise, otherwise, it is to find the critical difference between the two faces of the plate ( *T<sub>c</sub>* - *T<sub>m</sub>* ), notated as Δ*T*<sub>L</sub><sup>cr</sup> and Δ*T*<sub>N</sub><sup>cr</sup> for the cases of linearly and non-linearly distributed temperature, respectively. In the literature, the nonlinear *T*<sub>(*z*)</sub> is often approximated as a summation of a polynomial series as given by Javaheri and Eslami [29]. The more terms in the series the more accurate is the obtained temperature distribution. However, only the first seven terms are often included. The plot in Fig. 5 shows the nonlinear temperature distribution through the thickness of the Al/Al<sub>2</sub>O<sub>3</sub> FGM plate having the properties shown in Table 1, gradient index *n* = 2, a metallic bottom at ( *T<sub>m</sub>* °C ), and a ceramic top at ( *T<sub>c</sub>* °C ). Note that using two terms gives the linear distribution of the temperature. The figure shows a significant difference in the temperature distribution between the seven-term approximate series solution and the more accurate converged one. The plot also shows that the polynomial series solution converges to the numerical integration solution shown in eq. (35).

The relation between the number of terms in the polynomial series and the average error in temperature distribution through the thickness for various values of the gradient index *n* is presented by the semi-logarithmic plot in Fig. 6, which shows that as using more terms the approximate series solution converges. Note that the average error vanishes when (*n* = 0) or (*n* = ∞) as the material becomes pure ceramic or metallic, respectively, thus the temperature distribution becomes linear. The average percentage error plotted in Fig. 6 is calculated as follows.

$$\text{Average percentage error} = 100\% \times \left( \int_{-h/2}^{h/2} [T_{(z)}] dz - \int_{-h/2}^{h/2} [\hat{T}_{(z)}] dz \right) / ((T_c - T_m) h)
 \tag{36}$$

where  $\hat{T}_{(z)}$  is the integration solution shown in eq. (35). The temperature distribution through the thickness of an Al/Al<sub>2</sub>O<sub>3</sub> FGM plate as a function of the gradient index *n* is shown by the equally spaced contours of the semi-logarithmic plot in Fig. 7. That is, the temperature difference is the same between each two consequent contour lines. The figure shows that very low values as well as very high values of *n* lead to a roughly linear distribution of the temperature. Clearly, the moderate values of *n* lead to a nonlinear variation of the temperature through the thickness. That is understandable as for the very low and very high values of *n* the material becomes almost homogeneous ceramic or metallic, respectively.



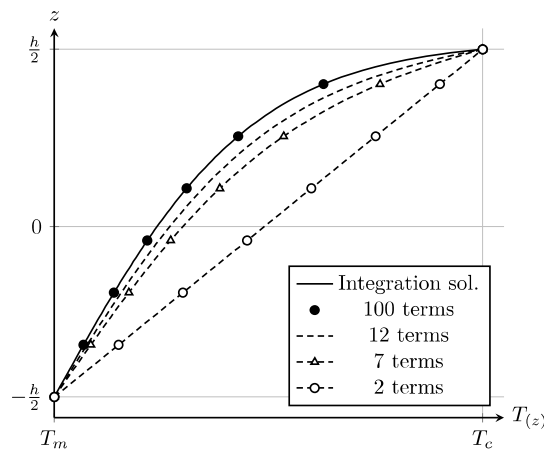


Fig. 5. Nonlinear temperature distribution through the thickness of the Al /Al<sub>2</sub>O<sub>3</sub> FGM plate having n=2, with respect to the number of terms in the approximate series solution

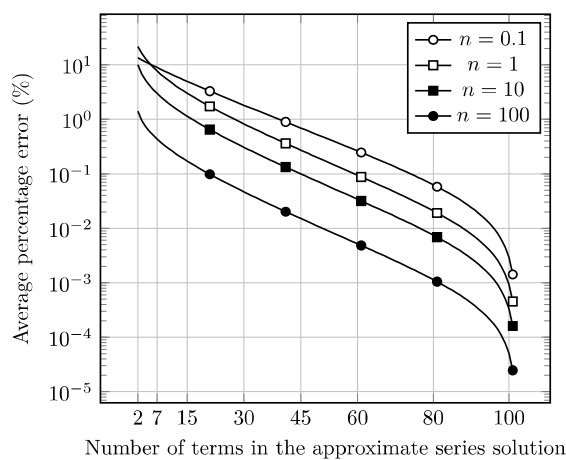


Fig. 6. Average percentage error of approximate temperature distribution through the thickness of the Al /Al<sub>2</sub>O<sub>3</sub> FGM plate with respect to the number of terms in the approximate series solution and the gradient index n

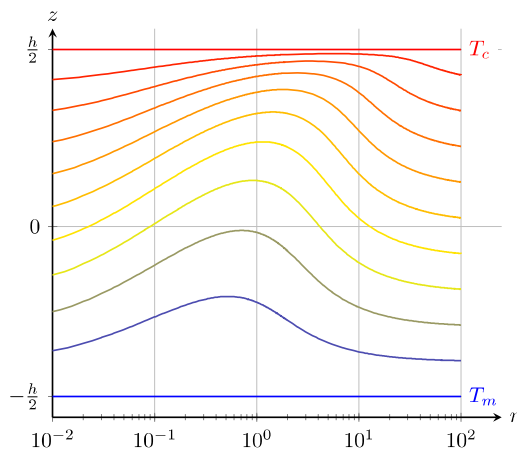


Fig. 7. Temperature distribution through the thickness of the Al /Al<sub>2</sub>O<sub>3</sub> FGM plate as a function of the gradient index n. (The contour lines are equally spaced)

### 6. ANSYS Finite Element Model

In addition to the analytical and numerical solutions found in the literature, EKM results are also compared to those obtained using the finite element method (FEM). FEM is implemented using ANSYS Mechanical APDL software. The finite element models of the FGM plate and the elastic foundation are as described in [25, 27, 51].

The plate model is meshed as 100 elements per edge, which is found fine enough to obtain the converged results. The variation of the properties through the thickness of the FGM material is modeled by considering the plate as a lamina, in which each laminate has its properties as a function of its position through the thickness. It is found that using 80 layers is well enough to obtain the converged result while being reasonably practical in terms of computational times.



**Table 2.** Critical uniform temperature rise of square SSSS Al /Al<sub>2</sub>O<sub>3</sub> FGM thin plate ( $a / h = 100$ ) with respect to  $n$

Method	Plate model	Gradient index $n$					
		0	0.5	1	2	5	10
EKM	CPT	17.0991	9.6879	7.9438	7.0426	7.2657	7.4692
Galerkin [29]	CPT	17.0991	9.6879	7.9438	7.0426	7.2657	7.4692
	IGA [52]	17.0946	9.6942	7.9557	7.0382	7.2555	-
ANSYS (FEM)	FSDT	17.0895	9.6831	7.9401	7.0402	7.2715	7.4753
Galerkin [30]	HSDT	17.0895	9.6831	7.940	7.0390	7.2607	7.4634

**Table 3.** Critical uniform temperature rise of square SSSS Al /Al<sub>2</sub>O<sub>3</sub> FGM moderately thick plate ( $a / h = 50$ ) with respect to  $n$

Method	Plate model	Gradient index $n$					
		0	0.5	1	2	5	10
EKM	CPT	68.3962	38.7515	31.7751	28.1704	29.0628	29.8771
Galerkin [29]	CPT	68.3964	38.7516	31.7751	28.1704	29.0629	29.8771
	IGA [52]	68.2429	38.7481	31.7874	29.1780	29.0875	-
ANSYS (FEM)	FSDT	68.2425	38.6749	31.7151	28.1170	29.0240	29.8304
Galerkin [30]	HSDT	68.2425	38.6751	31.7149	28.1131	28.9821	29.7837

**Table 4.** Critical uniform temperature rise of square CCCC Al /Al<sub>2</sub>O<sub>3</sub> FGM thin plate ( $a / h = 100$ ) with respect to  $n$

Method	Plate model	Gradient index $n$				
		0	0.5	1	2	5
EKM	CPT	45.24	25.67	21.06	18.50	19.25
Galerkin-power series [53]	CPT	45.51	25.79	21.15	18.75	19.34
Element-free [54]	FSDT	44.17	24.90	20.77	18.48	19.15
FEM [32]	FSDT	47.50	26.54	21.70	19.18	19.70
Galerkin [45]	HSDT	45.28	25.65	21.04	18.65	19.23
ANSYS (FEM)	FSDT	45.26	25.52	21.01	18.70	19.35

**Table 5.** Critical uniform temperature rise of square CCCC Al /Al<sub>2</sub>O<sub>3</sub> FGM moderately thick plate ( $a / h = 50$ ) with respect to  $n$

Method	Plate model	Gradient index $n$				
		0	0.5	1	2	5
EKM	CPT	181.757	102.979	84.440	74.860	77.232
Galerkin-power series [53]	CPT	182.06	103.15	84.58	74.99	77.36
Element-free [54]	FSDT	175.82	99.16	82.35	71.01	74.59
FEM [32]	FSDT	188.28	105.27	86.07	76.07	78.06
Galerkin [45]	HSDT	180.30	102.23	83.84	74.30	76.50
ANSYS (FEM)	FSDT	180.13	101.63	83.68	74.43	76.88

## 7. Validation of the Method

The derived stability equations are validated by comparing the results with the analytical and numerical solutions found in the literature in addition to the FEM solutions of ANSYS using the model described in Section 6. All the results in this study are obtained considering the material as Al /Al<sub>2</sub>O<sub>3</sub> FGM that is described in Section 4. Note that a large enough number of EKM terms  $t$  are used in obtaining the converged results presented here. The convergence study of the method with respect to the number of terms  $t$  is the exact same as the one presented in [27].

### 7.1 Uniform temperature rise

The buckling analysis of a square thin and a moderately thick FGM plate under uniform temperature rise is conducted first, then the buckling analysis of a thin plate with different values of the aspect ratio, and lastly, the buckling analysis of skew thin SSSS FGM. For the first case of square FGM thin ( $a / h = 100$ ) and moderately thick ( $a / h = 50$ ) plates, both simply supported SSSS and clamped CCCC FGM are considered. The results are compared with solutions of other methods found in the literature. In Tables (2 and 3), EKM results of the critical uniform temperature for thin and moderately thick SSSS FGM plates are compared with ANSYS (FEM), isogeometric analysis (IGA) [52] and Galerkin method [29, 30].

Note that those solutions are based on different plate theories. For instance, the FEM solutions of ANSYS and the IGA solutions at [52] are based on the first-order shear deformation theory (FSDT), while the Galerkin solutions at [29] are based on the classical plate theory (CPT) and the Galerkin solutions at [30] are based on the higher-order shear deformation theory (HSDT). The same comparison is conducted for the case of the SSSS FGM plates and presented in Tables (4 and 5). The second considered case is the rectangular SSSS Al /Al<sub>2</sub>O<sub>3</sub> thin FGM plates with different values of aspect ratio ( $b / a$ ) under uniform temperature rise. EKM results are compared to others in Table 6. In both cases, EKM is found to be very accurate in obtaining the critical temperatures of rectangular FGM plates under uniform temperature rise. Table 7 shows the good accuracy of EKM in finding the critical temperatures for skew plates as well. A more detailed investigation of the accuracy and convergence of the EKM with respect to the skew angle of the plate and the number of EKM terms  $i$  can be found in [27]. In all of the cases, EKM is found to be very accurate in obtaining the critical temperatures of FGM plates under uniform temperature rise.

### 7.2 Linear temperature rise

The buckling under linearly distributed temperature through the thickness of a square SSSS FGM plates with different values of the length-to-thickness ratio is conducted first, then the buckling analysis of thin SSSS FGM plates with different values of the aspect ratio, and lastly, the buckling analysis of skew thin SSSS FGM. Tables (8 and 9) show the EKM results compared to other solutions for different values of the length-to-thickness ratio ( $a / h$ ) and aspect ratio ( $b / a$ ), respectively.

Note that the results shown in Table 9 are obtained considering  $T_m$  being zero. Table 10 is listing the critical temperature rise for the thin skew FGM plate having  $a = b$ , under linearly distributed temperature, obtained using EKM, and compared to the element-free Galerkin's solution (EFG) of [31] and the FEM solutions of ANSYS. In Table 9, the results assigned to the references [29] and [30] are obtained using their presented solution equations with  $T_m = 0$ , which are numerically different from those listed there, i.e. in [29] and [30], where  $T_m = 5$  is considered. Also, note that the results in Tables (9 and 10) are obtained considering  $T_m = 5$ . In all of the considered cases, EKM shows high accuracy in obtaining the critical temperatures of rectangular FGM plates under linearly distributed temperature.



**Table 6.** Critical uniform temperature rise of the SSSS Al /Al<sub>2</sub>O<sub>3</sub> FGM thin plate with respect to *n* and *b / a*

n	Method	Plate model	Aspect ratio <i>b / a</i>			
			2	3	4	5
0	EKM	CPT	42.7478	85.4956	145.3423	222.2884
	Galerkin [29]	CPT	42.7478	85.4955	145.3424	222.2884
	ANSYS (FEM)	FSDT	42.7327	85.46876	145.2989	222.2232
	Galerkin [30]	HSDT	42.6876	85.2551	144.6490	220.6706
1	EKM	CPT	19.8594	39.7189	67.5221	103.2690
	Galerkin [29]	CPT	19.8594	39.7189	67.5221	103.2690
	ANSYS (FEM)	FSDT	19.8538	39.7090	67.5061	103.2452
	Galerkin [30]	HSDT	19.8359	39.6248	67.2507	102.6356
5	EKM	CPT	18.1643	36.3286	61.7586	94.4543
	Galerkin [29]	CPT	18.1643	36.3286	61.7586	94.4543
	ANSYS (FEM)	FSDT	18.1839	36.3700	61.8304	94.5651
	Galerkin [30]	HSDT	18.1327	36.2025	61.3952	93.6070
10	EKM	CPT	18.6732	37.3464	63.4888	97.1005
	Galerkin [29]	CPT	18.6732	37.3464	63.4888	97.1006
	ANSYS (FEM)	FSDT	18.6942	37.3910	63.5663	97.2202
	Galerkin [30]	HSDT	18.6367	37.2006	63.0687	96.1214

**Table 7.** Critical uniform temperature rise of skew SSSS Al /Al<sub>2</sub>O<sub>3</sub> thin FGM with respect to *n* and  $\phi$

n	Method	Plate model	Skew angle $\phi$			
			0°	15°	30°	45°
1	EKM	CPT	7.9438	8.4069	10.1355	14.1530
	ANSYS (FEM)	FSDT	7.9171	8.3693	9.9972	14.1049
5	EKM	CPT	7.2657	7.6897	9.1713	12.9205
	ANSYS (FEM)	FSDT	7.3044	7.7213	9.2199	12.9890

**Table 8.** Critical rise of linearly changing temperature across the thickness of SSSS Al /Al<sub>2</sub>O<sub>3</sub> FGM square, with respect to *n* and *a/h*. (*T<sub>m</sub>* = 0)

n	Method	Plate model	<i>a / h</i>			
			10	25	50	100
0	EKM	CPT	3419.8214	547.1714	136.7929	34.1982
	Galerkin [29]	CPT	3419.8213	547.1714	136.7929	34.1982
	ANSYS (FEM)	FSDT	3237.2481	542.2781	136.4850	34.1789
	Galerkin [30]	HSDT	3237.3638	542.27861	136.4850	34.1789
1	EKM	CPT	1489.8277	238.3724	59.5931	14.8983
	Galerkin [29]	CPT	1489.8277	238.3724	59.5931	14.8983
	ANSYS (FEM)	FSDT	1421.1020	236.3848	59.4326	14.8793
	Galerkin [30]	HSDT	1422.3454	236.5755	59.4802	14.8912
5	EKM	CPT	1250.6418	200.1027	50.0257	12.5064
	Galerkin [29]	CPT	1250.6418	200.1027	50.0257	12.5064
	ANSYS (FEM)	FSDT	1173.6360	198.9088	50.1517	12.5648
	Galerkin [30]	HSDT	1169.2917	197.8980	49.8867	12.4977
10	EKM	CPT	1323.6032	211.7765	52.9441	13.2360
	Galerkin [29]	CPT	1323.6032	211.7765	52.9441	13.2360
	ANSYS (FEM)	FSDT	1238.3031	211.1854	53.2981	13.3563
	Galerkin [30]	HSDT	1227.4996	209.1543	52.7787	13.2257

**Table 9.** Critical rise of linearly changing temperature across the thickness of SSSS Al /Al<sub>2</sub>O<sub>3</sub> FGM thin plate, with respect to *n* and *b/a*. (*T<sub>m</sub>* = 5)

n	Method	Plate model	<i>b / a</i>				
			1	2	3	4	5
0	EKM	CPT	24.198	75.496	160.991	280.685	434.577
	Galerkin [29]	CPT	24.198	75.495	160.991	280.684	434.576
	Galerkin [30]	HSDT	24.177	75.376	160.505	279.297	431.334
1	EKM	CPT	5.521	27.868	65.114	117.258	184.300
	Galerkin [29]	CPT	5.520	27.868	65.114	117.258	184.300
	Galerkin [30]	HSDT	5.513	27.823	64.936	116.748	183.110
5	EKM	CPT	3.900	22.660	53.926	97.698	153.977
	Galerkin [29]	CPT	3.899	22.659	53.925	97.698	153.977
	Galerkin [30]	HSDT	3.891	22.604	53.710	97.073	152.516
10	EKM	CPT	4.376	24.230	57.320	103.646	163.208
	Galerkin [29]	CPT	4.375	24.229	57.319	103.646	163.208
	Galerkin [30]	HSDT	4.364	24.165	57.061	102.901	161.471

**Table 10.** Critical rise of linearly changing temperature across the thickness of skew SSSS Al /Al<sub>2</sub>O<sub>3</sub> FGM plate, with respect to *n*, *a/b*, and  $\phi$ . (*T<sub>m</sub>*=5)

<i>a / b</i>	$\phi$	<i>n</i>					
		1			5		
		EKM (CPT)	EFG [31] (CPT)	FEM (FSDT)	EKM (CPT)	EFG [31] (CPT)	FEM (FSDT)
1	0°	5.5209	5.5199	5.5207	3.8999	3.8991	3.8987
	15°	6.3806	6.3133	6.4022	4.6252	4.5651	4.6385
	30°	9.5001	9.2260	9.7737	7.3198	7.6308	7.4681
	45°	17.6795	17.9718	19.0164	14.0963	14.3519	15.2242
2	0°	27.8683	27.8812	-	22.6594	22.6704	-
	15°	30.2000	30.1040	-	24.6168	24.5363	-
	30°	38.7561	38.2188	-	31.8156	31.7856	-
	45°	60.6512	60.4732	-	50.2507	50.0298	-

**7.3 Nonlinearly distributed temperature**

The buckling under nonlinearly distributed temperature through the thickness of a square SSSS FGM plates with different values of the length-to-thickness ratio is conducted first, then the buckling analysis of thin SSSS FGM plates with different values of the aspect ratio, and lastly, the buckling analysis of skew thin SSSS FGM. Tables (11 and 12) show the EKM results compared to



other solutions for different values of the length-to-thickness ratio ( $a/h$ ) and aspect ratio ( $b/a$ ), respectively. Table 13 is listing the critical temperature difference for the thin skew FGM plate having  $a = b$ , under nonlinearly distributed temperature, obtained using EKM, and compared to the element-free Galerkin's solution (EFG) of [31] and the FEM solutions of ANSYS. Note that the results shown in Tables (11 and 12) are obtained considering  $T_m = 5$ . Both the converged and the seven-term polynomial series solutions of the nonlinear distribution of the temperature through the thickness are considered. Both Table 11 and Table 12 show the significant difference in the resulting buckling temperature between the two cases. In all the considered cases, EKM shows high accuracy in obtaining the critical temperatures of rectangular FGM plates under nonlinearly distributed temperature.

### 8. Relations between the Critical Temperatures

The numerical results obtained below are all for a thin fully simply supported Al/Al<sub>2</sub>O<sub>3</sub> FGM plate, width  $b = 1m$ , and length-to-thickness ratio  $a/h = 100$ , resting on the Pasternak elastic foundation. Conventionally, the stiffness of the elastic foundation is expressed in a non-dimensional form as

$$k_n^* = \frac{k_n a^4}{100D} \quad k_p^* = \frac{k_p a^2}{100D} \tag{37}$$

where  $a$  is the half of the length of the plate.  $k_n$  is the out-of-plane extension stiffness coefficient in the units of the load over the unit area for the unit lateral deflection of that area ( $N/m^2/m$ ),  $k_p$  is the shear stiffness coefficient in the units of the load over unit in-plane shearing ( $N/m$ ),  $k_n^*$  and  $k_p^*$  are the non-dimensional forms of  $k_n$  and  $k_p$ , respectively. In this section, only fully supported plates are considered. However, the same relations must be true for the cases of clamped plates and plates with any combinations of simply supported and clamped edges. Fig. 8 shows the thermal buckling of the plate under uniform temperature rise ( $\Delta T_U^c$ ), linear ( $\Delta T_L^c$ ) and nonlinear ( $\Delta T_N^c$ ) temperature change across the thickness, with respect to the aspect ratio  $a/b$  for different values of the parameters of Pasternak elastic foundation  $k_n^*, k_p^*$ .

**Table 11.** Critical rise of nonlinearly changing temperature across the thickness of SSSS Al/Al<sub>2</sub>O<sub>3</sub> FGM square plate, with respect to  $n$  and  $a/h$ . ( $T_m = 5$ )

n	Method	Terms in $T(z)$	Plate model	$a/h$					
				10	20	40	60	80	100
0	EKM	100	CPT	3409.821	844.955	203.739	84.995	43.435	24.198
	EKM	7	CPT	3409.821	844.955	203.739	84.995	43.435	24.198
	Galerkin [29]	7	CPT	3409.821	844.955	203.738	84.995	43.434	24.198
	Galerkin [30]	7	HSDT	3224.968	833.032	202.984	84.848	43.387	24.177
1	EKM	100	CPT	2633.408	645.842	148.950	56.933	24.727	9.821
	EKM	7	CPT	2055.001	503.988	116.235	44.428	19.296	7.664
	Galerkin [29]	7	CPT	2055.001	503.987	116.234	44.428	19.296	7.663
	Galerkin [30]	7	HSDT	1960.018	497.903	115.849	44.352	19.270	7.652
5	EKM	100	CPT	1749.960	428.396	98.004	36.821	15.407	5.495
	EKM	7	CPT	1553.336	380.261	86.993	32.684	13.675	4.877
	Galerkin [29]	7	CPT	1553.336	380.261	86.999	32.683	13.675	4.877
	Galerkin [30]	7	HSDT	1450.769	373.557	86.568	32.600	13.648	4.866
10	EKM	100	CPT	1633.873	400.210	91.794	34.680	14.690	5.438
	EKM	7	CPT	1519.568	372.211	85.372	32.254	13.663	5.057
	Galerkin [29]	7	CPT	1519.568	372.211	85.372	32.254	13.662	5.057
	Galerkin [30]	7	HSDT	1408.132	364.857	84.905	32.162	13.634	5.044

**Table 12.** Critical rise of nonlinearly changing temperature across the thickness of SSSS Al/Al<sub>2</sub>O<sub>3</sub> FGM thin plate, with respect to  $n$  and  $b/a$ . ( $T_m = 5$ )

n	Method	Terms in $T(z)$	Plate model	$b/a$				
				1	2	3	4	5
0	EKM	100	CPT	24.198	75.496	160.991	280.685	434.577
	EKM	7	CPT	24.198	75.496	160.991	280.685	434.577
	Galerkin [29]	7	CPT	24.198	75.495	160.991	280.684	434.576
	Galerkin [30]	7	HSDT	24.177	75.376	160.505	279.297	431.334
1	EKM	100	CPT	9.821	49.572	115.824	208.577	327.831
	EKM	7	CPT	7.664	38.684	90.384	162.765	255.826
	Galerkin [29]	7	CPT	7.663	38.683	90.384	162.764	255.825
	Galerkin [30]	7	HSDT	7.652	38.622	90.138	162.057	254.174
5	EKM	100	CPT	5.495	31.926	75.978	137.651	216.945
	EKM	7	CPT	4.877	28.339	67.441	122.185	192.569
	Galerkin [29]	7	CPT	4.877	28.338	67.441	122.184	192.569
	Galerkin [30]	7	HSDT	4.866	28.270	67.172	121.403	190.743
10	EKM	100	CPT	5.438	30.111	71.233	128.804	202.824
	EKM	7	CPT	5.057	28.005	66.250	119.793	188.634
	Galerkin [29]	7	CPT	5.057	28.004	66.249	119.793	188.634
	Galerkin [30]	7	HSDT	5.044	27.929	65.951	118.932	186.627

**Table 13.** Critical rise of nonlinearly changing temperature across the thickness of skew SSSS Al/Al<sub>2</sub>O<sub>3</sub> FGM thin plate, with respect to  $n$ ,  $a/b$ , and  $\phi$ . ( $T_m = 5$ )

$a/b$	$\phi$	n					
		1			5		
		EKM (CPT)	EFG [31] (CPT)	FEM (FSDT)	EKM (CPT)	EFG [31] (CPT)	FEM (FSDT)
1	0°	7.6636	7.6621	7.6632	4.8774	4.8763	4.8758
	15°	8.8903	8.7634	8.8869	5.7865	5.7093	5.8011
	30°	13.1818	12.8065	13.5668	10.0054	9.5433	9.3399
	45°	24.5723	24.9465	26.3965	17.6529	17.9490	19.0400
2	0°	38.6838	38.7017	38.6525	28.3389	28.3524	28.3067
	15°	41.9188	41.7871	41.9254	30.7883	30.6860	30.7810
	30°	53.7081	53.0512	54.0838	39.6498	39.7522	39.9718
	45°	85.2902	83.9423	85.5235	62.7607	62.5692	63.7321



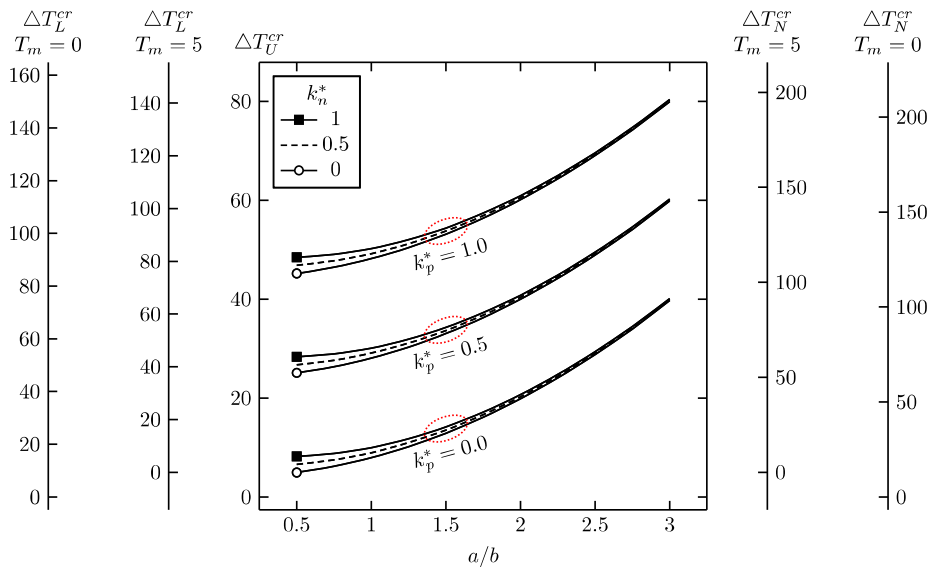


**Fig. 8.** Critical temperature rise of thin rectangular SSSS Al/Al<sub>2</sub>O<sub>3</sub> FGM plate having  $n = 1$ ,  $b = 1\text{m}$ , and  $a/h=100$  under various temperature distributions across the thickness, with respect to  $a/b$ ,  $T_m$ ,  $k_n$ , and  $k_p$

Note that  $T_m = 0\text{ }^\circ\text{C}$  and  $T_m = 5\text{ }^\circ\text{C}$  are both used in each of the cases of linear and nonlinear temperature distributions. It is found that the results of the three cases of different temperature distributions produce the exact same plot but with different scales. It is also notable that the results in the cases of  $T_m = 0\text{ }^\circ\text{C}$  and the corresponding ones of  $T_m = 5\text{ }^\circ\text{C}$  are linearly related by a just an offset. The zero values of the critical temperature rise in **Fig. 8** for the cases of the linear and nonlinear temperature distributions indicate that the uniform part  $T_m$  of the thermal load is just enough by its own to cause the buckling. These linear relations between the buckling temperatures of the FGM plate under various types of temperature distribution can be reasoned as follows. The only term that is derived from the temperature distribution is the force resultant of the thermal load  $N_T$ . So, the critical temperature is the one that produces the critical thermal force resultant  $N_T^{cr}$ . In the case of uniform temperature rise, shown in eq. (33), the temperature distribution becomes a constant ( $T(z) = T_m$ ). Substituting the buckling uniform temperature  $\Delta T_U^{cr}$  in eq. (21) gives  $N_T^{cr}$ .

$$N_T^{cr} = \int_{-h/2}^{h/2} [\hat{\mu} E_{(z)} \alpha_{(z)} \Delta T_U^{cr}] dz = \Delta T_U^{cr} \int_{-h/2}^{h/2} [\hat{\mu} E_{(z)} \alpha_{(z)}] dz = \Delta T_U^{cr} C_1 \tag{38}$$

where  $\hat{\mu}$  is as defined in eq. (22). When the temperature is linearly distributed through the thickness, as shown in eq. (33), the critical temperature difference  $\Delta T_L^{cr}$  between the ceramic and metallic surfaces ( $T_c - T_m$ ) is obtained by substituting  $\Delta T_L^{cr}$  in eq. (33) and then in eq. (21) gives

$$N_T^{cr} = \int_{-h/2}^{h/2} \left[ \hat{\mu} E_{(z)} \alpha_{(z)} \left( T_m + \Delta T_L^{cr} \left( \frac{z}{h} + \frac{1}{2} \right) \right) \right] dz = \Delta T_L^{cr} C_2 + T_m C_1 \tag{39}$$

Comparing eq. (38) with eq. (39) gives

$$\Delta T_L^{cr} = \frac{C_1}{C_2} (\Delta T_U^{cr} - T_m) \tag{40}$$

where  $C_1$  and  $C_2$  are constants given as

$$C_1 = \int_{-h/2}^{h/2} [\hat{\mu} E_{(z)} \alpha_{(z)}] dz \quad C_2 = \int_{-h/2}^{h/2} \left[ \hat{\mu} E_{(z)} \alpha_{(z)} \left( \frac{z}{h} + \frac{1}{2} \right) \right] dz \tag{41}$$

In the case of nonlinear temperature distribution, shown in eq. (21), the critical temperature difference  $\Delta T_N^{cr}$  between the ceramic and metallic surfaces ( $T_c - T_m$ ) is obtained from eq. (21) as

$$N_T^{cr} = \int_{-h/2}^{h/2} \left[ \hat{\mu} E_{(z)} \alpha_{(z)} \left( T_m + \Delta T_N^{cr} \frac{K^v(z)}{K^c} \right) \right] dz \tag{42}$$

Comparing eq. (38) with eq. (42) gives

$$\Delta T_N^{cr} = \frac{K^c C_1}{C_3} (\Delta T_U^{cr} - T_m) \tag{43}$$

where the function  $K^v(z)$  and the constants  $K^c$  and  $C_3$  are given as



$$K^c = \int_{-h/2}^{h/2} \left[ \frac{1}{K(z)} \right] dz \quad K_{(z)}^v = \int_{-h/2}^z \left[ \frac{1}{K(z)} \right] dz \quad C_3 = \int_{-h/2}^{h/2} [\hat{\mu} E_{(z)} \alpha_{(z)} K_{(z)}^v] dz \quad (44)$$

By using the derived relations in eq. (40) and eq. (43), the critical temperature of the same FGM plate under any temperature distribution can be obtained from any given one. eq. (40) can be further simplified by substituting the assumed variation of properties, then becomes as follows.

$$\Delta T_U^c = 2 \left( \frac{\frac{\alpha_{cm} E_m + \alpha_m E_{cm}}{n+1} + \frac{\alpha_{cm} E_{cm} + \alpha_m E_m}{2n+1}}{\frac{2(\alpha_{cm} E_m + \alpha_m E_{cm})}{n+2} + \frac{\alpha_{cm} E_{cm} + \alpha_m E_m}{n+1}} \right) (\Delta T_U^c - T_m) \quad (45)$$

This simplification could not be implemented to the nonlinear temperature distribution of eq. (43), because no simple analytical solutions are found for the integrals  $C_3$  and  $K^c$ .

The same linear relations are also noticed when using any other material gradient index  $n$ . To show this the same analysis is conducted for the Al /Al<sub>2</sub>O<sub>3</sub> FGM plate but with different material gradient index,  $n = 2$ . From the results in **Fig. 9**, it is found that the exact plot also results, but again in different linear scales. So the linear transformations shown in eq. (45) and eq. (43) are valid for any value of the material gradient index  $n$ .

The same analysis is again conducted for the thin Al /Al<sub>2</sub>O<sub>3</sub> FGM plate having  $n = 1$ , but with skew angle  $\psi = 30^\circ$ . The results in **Fig. 10** show that the critical temperatures are also linearly related for the skew FGM plates, as it is found that the exact plot also results, but again in different linear scales. The linear transformations in eq. (45) and eq. (43) are also valid for the skew thin FGM plates.

In addition, when comparing the critical temperatures of the two thin Al /Al<sub>2</sub>O<sub>3</sub> FGM plates having different material gradient indices  $n$  in **Fig. 8** and **Fig. 9** it can be easily noticed that the critical temperatures of the two cases are also linearly related. That is also noted for the case of the thin FGM skew plate, shown in **Fig. 10** and **Fig. 11**. The relation between the two cases of each FGM plate geometry can be derived from the stability equation eq. (30) by factoring out  $D$  and  $G_1$ , given that  $G_2$  vanishes since  $T_0$  is considered zero. For the case of uniform thermal load, the relation between the critical uniform temperatures  $\Delta T_{U_1}^c$  of a particular thin FGM plate can be obtained from the critical uniform temperature rise  $\Delta T_{U_2}^c$  of any other plate with the same dimensions and boundary conditions but different materials using the equation below.

$$\frac{N_{uT_1}}{D_1} \Delta T_{U_1}^c = \frac{N_{uT_2}}{D_2} \Delta T_{U_2}^c \quad (46)$$

where the numeric subscripts "1" and "2" indicate the first and second FGM plates.  $N_{uT}$  is the resultant force from unit temperature rise, i.e.

$$N_{uT} = \int_{-h/2}^{h/2} [\hat{\mu} E_{(z)} \alpha_{(z)}] dz \quad (47)$$

By using the linear transformations in eq. (45), eq. (43), and eq. (46), with only one known critical temperature of a particular FGM plate, all other critical temperatures can be obtained not only for that particular FGM plate but also for any other plate with the same dimensions and boundary conditions. The relations of the critical temperatures to the two parameters of the Pasternak elastic foundation are investigated. For the rectangular thin FGM plates, **Fig. 8** and **Fig. 9** show that regardless of the material of the plate, the shear stiffness  $k_p$  linearly scales the critical temperatures. From the stability equations, for two thin plates of the same materials resting on the Pasternak elastic foundation with different shear stiffness  $k_p$  the critical uniform temperatures are related by the following equation.

$$N_{uT_1} \Delta T_{U_1}^c - k_{p_1} = N_{uT_2} \Delta T_{U_2}^c - k_{p_2} \quad (48)$$

For the case of the skew plates, **Fig. 10** and **Fig. 11** show that  $k_p$  does not linearly scale the critical temperatures anymore. Since this work is focusing only on the linear relations, the effect of  $k_p$ , in this case, is not further investigated. In both **Fig. 10** and **Fig. 11**, the effect of the normal stiffness  $k_n$  of the Pasternak elastic foundation is found linear and decreasing as the aspect ratio  $a/b$  increases. Although  $k_n$  has a linear effect on the critical temperatures, it is found that there is no simple way to formulate this relation. It is found that the effect of the elastic foundations on the critical temperatures of a skew FGM plate is not easily described by linear relations. However, the linear relations between the different cases of temperature distributions are still the same as those for the rectangular plate, which are shown in eq. (40) and eq. (43).

In addition, comparing **Fig. 10** with **Fig. 11** shows the linear relation between the critical temperatures of different FGM skew plates having the same dimensions, boundary conditions and skew angle under the same temperature distributions. This linear relation is the same as the one of the rectangular plates shown in eq. (46).

One last important linear relation to mention is the effect of the square of the length-to-thickness ratio  $a/h$  on the critical temperature under various temperature distribution. As Table 8 shows, the square of the length-to-thickness ratio scales the critical temperatures by simple multiplication, given that  $T_m = 0$ . For two thin plates having the same material, boundary conditions, and aspect ratio  $a/b$  but different length-to-thickness ratio  $a/h$  with  $T_m = 0$ , the critical temperatures of them are related as follows.



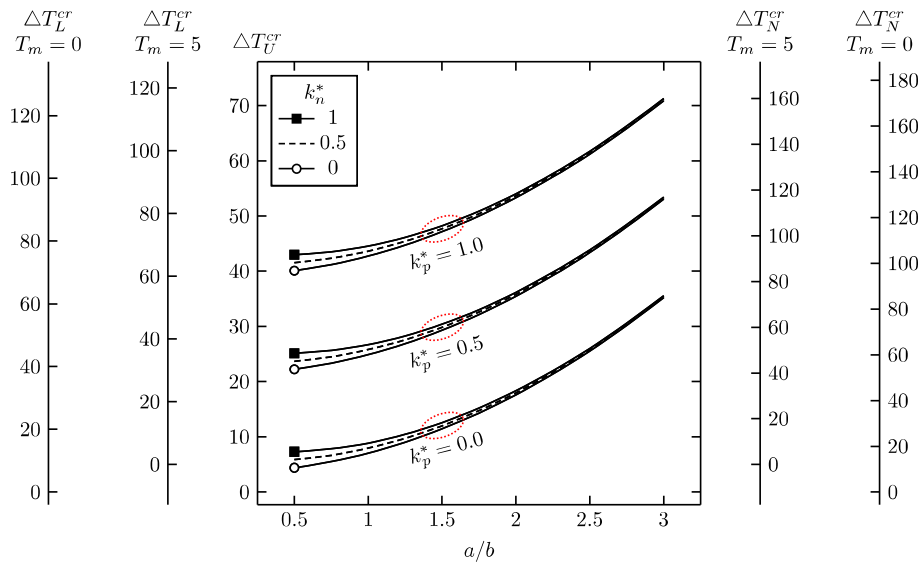


Fig. 9. Critical temperature rise of thin rectangular SSSS Al/Al<sub>2</sub>O<sub>3</sub> FGM plate having  $n = 2$ ,  $b = 1m$ , and  $a/h=100$  under various temperature distributions across the thickness, with respect to  $a/b$ ,  $T_m$ ,  $k_n^*$ , and  $k_p^*$

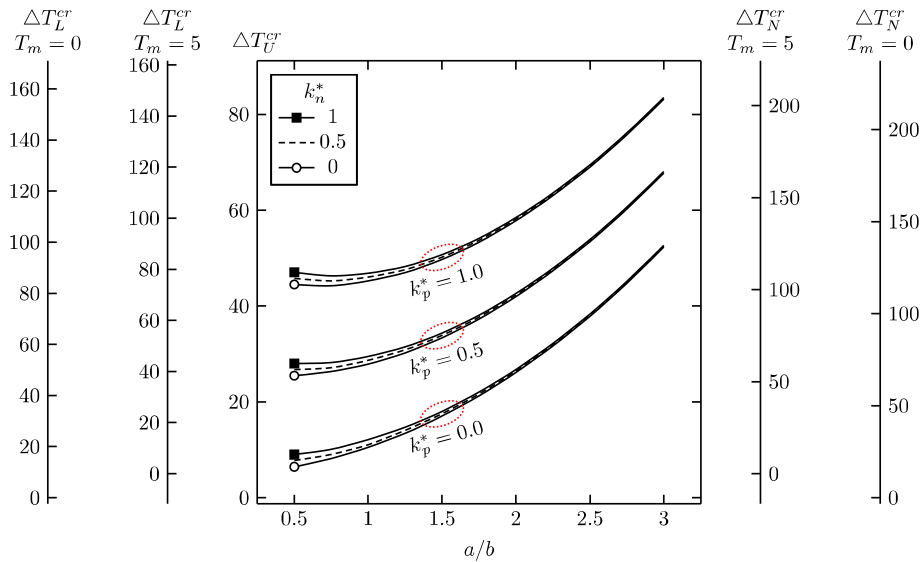


Fig. 10. Critical temperature rise of thin skew SSSS Al/Al<sub>2</sub>O<sub>3</sub> FGM plate having  $n = 1$ ,  $b = 1m$ ,  $\phi = 30^\circ$ , and  $a/h=100$  under various temperature distributions across the thickness, with respect to  $a/b$ ,  $T_m$ ,  $k_n^*$ , and  $k_p^*$

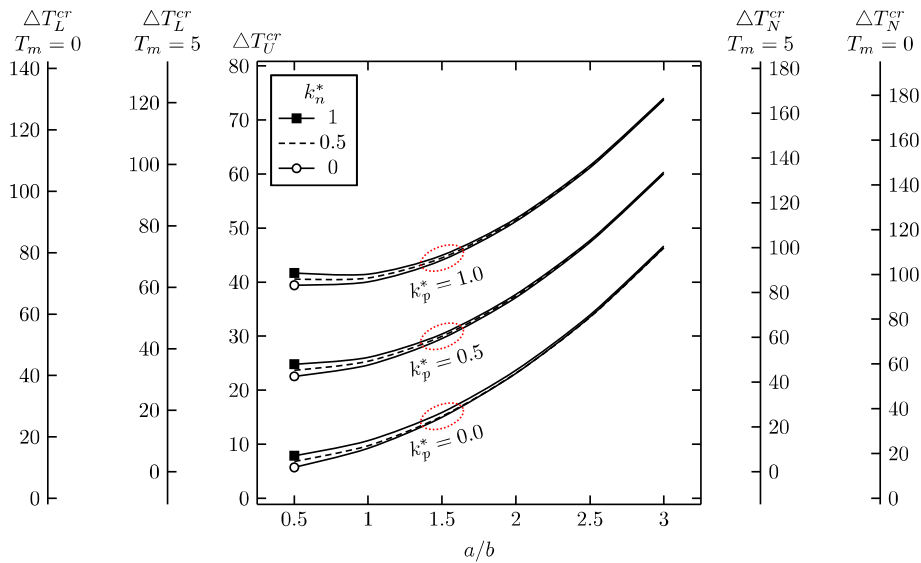


Fig. 11. Critical temperature rise of thin skew SSSS Al/Al<sub>2</sub>O<sub>3</sub> FGM plate having  $n = 2$ ,  $b = 1m$ ,  $\phi = 30^\circ$ , and  $a/h=100$  under various temperature distributions across the thickness, with respect to  $a/b$ ,  $T_m$ ,  $k_n^*$ , and  $k_p^*$



$$\Delta T_1^{cr} (a_1 / h_1)^2 = \Delta T_2^{cr} (a_2 / h_2)^2 \quad (49)$$

Caution must be taken when implementing eq. (49) by considering only thin plates, i.e. larger values of the length-to-thickness ratio  $a/h$ , as the derived formulae are all based on the classical plate theory.

## 9. Conclusion

The relations between the critical temperatures of the thin FGM plates under various temperature distributions through the thickness of FGM plate resting on the Pasternak elastic foundation have been investigated. Both rectangular and skew plates are considered. Formulations are derived based on the classical plate theory (CPT) considering the von Karman nonlinearities and taking the physical neutral plane as the reference plane. By using the multi-term extended Kantorovich method (EKM) the stability equations and boundary conditions terms are derived according to Trefftz criteria of the minimum total potential energy using the variational calculus expressed in an oblique coordinate system. The nonlinearly distributed temperature is obtained by solving the heat conduction problem. The obtained formulations are validated by comparison with the analytical and numerical solutions found in the literature, and to the finite element solutions obtained using ANSYS software. Novel multi-scale plots are used to illustrate the linear relations between critical temperatures under various temperature distributions. It is found that the critical temperatures of a particular thin FGM plate under uniformly, linearly, and nonlinearly distributed temperature through the thickness are all linearly related. In addition, the critical temperatures of thin FGM plates of different materials but having the same dimensions and boundary conditions are found also linearly related. These are found true for the skew FGM plates as well. The shear stiffness of the Pasternak foundation is found to linearly scale the critical temperature of the thin rectangular FGM plate, but not the skew ones. The normal stiffness of the Pasternak foundation is found to linearly scale the critical temperature of both the thin rectangular and skew FGM plates, but its effect decreases as the aspect ratio increases. Lastly, the squared length-to-thickness ratio is also found to linearly scale the critical temperatures of the thin FGM plate. It can be concluded that, by knowing one critical temperature for a thin FGM plate under specific temperature distribution, all other critical temperatures not only for this particular plate but also for any other thin FGM plate of different materials with the same in-plane dimensions and boundary conditions can be obtained by the derived simple linear relations. One benefit of these linear relations derived here is the speed it provides, which can be crucial in the optimization studies. The following investigations may be on the relations between the critical temperatures of thick plates based on higher-shear deformation theories.

## Author Contributions

A.H.A. Hassan developed the mathematical modeling, programmed the EKM method in MATLAB, conducted the comparisons in tables and figures, and wrote and revised the manuscript; N. Kurgan planned the scheme, initiated the project, and suggested the experiments; N. Can conducted the finite element analysis in ANSYS APDL. The manuscript was written through the contribution of all authors. All authors discussed the results, reviewed, and approved the final version of the manuscript.

## Conflict of Interest

The authors declared no potential conflicts of interest with respect to the research, authorship, and publication of this article.

## Funding

The authors received no financial support for the research, authorship, and publication of this article.

## References

- [1] Shen, M., and Bever, M., Gradients in polymeric materials, *Journal of Materials science*, 7(7), 1972, 741-746.
- [2] Bever, M., and Duwez, P., Gradients in composite materials, *Materials Science and Engineering*, 10, 1972, 1-8.
- [3] Hassan Ahmed Hassan, A., and Kurgan, N., A Review on buckling analysis of functionally graded plates under thermo-mechanical loads, *International Journal of Engineering & Applied Sciences*, 11(1), 2019, 345-368.
- [4] Ichikawa, K., *Functionally graded materials in the 21st century: a workshop on trends and forecasts*, Springer Science & Business Media, 2001.
- [5] Singh, A. K., Noise Emission from Functionally Graded Materials based Polypropylene Spur Gears-A Tribological Investigation, *Materials Today: Proceedings*, 5(2), 2018, 8199-8205.
- [6] Singh, A. K., A novel technique for in-situ manufacturing of functionally graded materials based polymer composite spur gears, *Polymer Composites*, 40(2), 2019, 523-535.
- [7] Tian, X., Zhao, J., Yang, H., Wang, Z., and Liu, H., High-speed intermittent turning of GH2132 alloy with Si 3 N 4/(W, Ti) C/Co graded ceramic tool, *International Journal of Advanced Manufacturing Technology*, 100(1-4), 2019, 401-408.
- [8] Nguoyep, L. L. M., Ndop, J., Nkene, E. R. A., and Ndjaka, J.-M. B., Numerical and Analytical Calculations for Modeling and Designing Drilling Wicks or Rotary Cutters Based of Functionally Graded Materials, *Journal of Engineering*, 2018, 2018.
- [9] Nikbakht, S., Kamarian, S., and Shakeri, M., A review on optimization of composite structures Part II: Functionally graded materials, *Composite Structures*, 214, 2019, 83-102.
- [10] El-Galy, I., Saleh, B., and Ahmed, M., Functionally graded materials classifications and development trends from industrial point of view, *SN Applied Sciences*, 1(11), 2019, 1-23.
- [11] Reddy, J. N., *Theory and analysis of elastic plates and shells*, CRC press, 2006.
- [12] Cuba, L., Arciniega, R., and MANTARI, J. L., Generalized 2-Unknown's HSDT to Study Isotropic and Orthotropic Composite Plates, *Journal of Applied and Computational Mechanics*, 5(1), 2019, 141-149.
- [13] Zenkour, A. M., Hafed, Z. S., and Radwan, A. F., Bending Analysis of Functionally Graded Nanoscale Plates by Using Nonlocal Mixed Variational Formula, *Mathematics*, 8(7), 2020, 1162.
- [14] Sobhy, M., and Zenkour, A. M., A comprehensive study on the size-dependent hygrothermal analysis of exponentially graded microplates on elastic foundations, *Mechanics of Advanced Materials and Structures*, 27(10), 2020, 816-830.
- [15] Jena, S. K., Chakraverty, S., Malikan, M., and Sedighi, H. M., Implementation of Hermite-Ritz method and Navier's technique for vibration of functionally graded porous nanobeam embedded in Winkler-Pasternak elastic foundation using bi-Helmholtz nonlocal elasticity, *Journal of Mechanics of Materials and Structures*, 15(3), 2020, 405-434.
- [16] Sgouros, A. P., Kalosakas, G., Papagelis, K., and Galiotis, C., Compressive response and buckling of graphene nanoribbons, *Scientific Reports*, 8(1), 2018, 9593.
- [17] Zarei, M., Faghani, G., Ghalami, M., and Rahimi, G. H., Buckling and Vibration Analysis of Tapered Circular Nano Plate, *Journal of Applied and Computational Mechanics*, 4(1), 2018, 40-54.
- [18] Ventsel, E., Krauthammer, T., and Carrera, E., Thin plates and shells: theory, analysis, and applications, *Applied Mechanics Reviews*, 55(4), 2002, B72-B73.



- [19] Srinivasa, C., Kumar, Y. S. W. P., and Banagar, A. R., Bending Behavior of Simply Supported Skew Plates, *Int. J. Sci. Eng. Res.*, 9, 2018, 21-26.
- [20] Monroe-Aerospace, "Why Do Airplanes Have Swept Wings?," 2019, <https://monroe-aerospace.com/blog/why-do-airplanes-have-swept-wings/>.
- [21] Shen, H.-S., and Wang, Z.-X., Nonlinear bending of FGM plates subjected to combined loading and resting on elastic foundations, *Composite Structures*, 92(10), 2010, 2517-2524.
- [22] Mahmoudi, A., Benyoucef, S., Tounsi, A., Benachour, A., Adda Bedia, E. A., and Mahmoud, S., A refined quasi-3D shear deformation theory for thermo-mechanical behavior of functionally graded sandwich plates on elastic foundations, *Journal of Sandwich Structures & Materials*, 21(6), 2019, 1906-1929.
- [23] Zhang, Y. F., and Liu, J. T., A widespread internal resonance phenomenon in functionally graded material plates with longitudinal speed, *Scientific Reports*, 9(1), 2019, 1907.
- [24] Menasria, A., Kaci, A., Bousahla Abdelmoumen, A., Bourada, F., Tounsi, A., Benrahou Kouider, H., Tounsi, A., Adda Bedia, E. A., and Mahmoud, S. R., A four-unknown refined plate theory for dynamic analysis of FG-sandwich plates under various boundary conditions, *Steel and Composite Structures*, 36(3), 2020, 355-367.
- [25] Hassan Ahmed Hassan, A., and Kurgan, N., Bending analysis of thin FGM skew plate resting on Winkler elastic foundation using multi-term extended Kantorovich method, *Engineering Science and Technology, an International Journal*, 23(4), 2020, 788-800.
- [26] Zine, A., Bousahla Abdelmoumen, A., Bourada, F., Benrahou Kouider, H., Tounsi, A., Adda Bedia, E. A., Mahmoud, S. R., and Tounsi, A., Bending analysis of functionally graded porous plates via a refined shear deformation theory, *Computers and Concrete*, 26(1), 2020, 63-74.
- [27] Hassan, A. H. A., and Kurgan, N., Buckling of thin skew isotropic plate resting on Pasternak elastic foundation using extended Kantorovich method, *Heliyon*, 6(6), 2020, e04236.
- [28] Rabhi, M., Benrahou, K. H., Kaci, A., Houari, M. S. A., Bourada, F., Bousahla, A. A., Tounsi, A., Bedia, E. A., Mahmoud, S., and Tounsi, A., A new innovative 3-unknowns HSDT for buckling and free vibration of exponentially graded sandwich plates resting on elastic foundations under various boundary conditions, *Geomechanics and Engineering*, 22(2), 2020, 119.
- [29] Javaheri, R., and Eslami, M., Thermal buckling of functionally graded plates, *AIAA Journal*, 40(1), 2002, 162-169.
- [30] Javaheri, R., and Eslami, M., Thermal buckling of functionally graded plates based on higher order theory, *Journal of Thermal Stresses*, 25(7), 2002, 603-625.
- [31] Saadatpour, M., Azhari, M., and Bradford, M., Buckling of arbitrary quadrilateral plates with intermediate supports using the Galerkin method, *Computer Methods in Applied Mechanics and Engineering*, 164(3-4), 1998, 297-306.
- [32] Nguyen-Xuan, H., Tran, L. V., Nguyen-Thoi, T., and Vu-Do, H., Analysis of functionally graded plates using an edge-based smoothed finite element method, *Composite Structures*, 93(11), 2011, 3019-3039.
- [33] Can, N., Kurgan, N., and Hassan Ahmed Hassan, A., Buckling Analysis of Functionally Graded Plates Using Finite Element Analysis, *International Journal of Engineering and Applied Sciences*, 12(1), 2020, 43-56.
- [34] Kerr, A. D., An extension of the Kantorovich method, *Quarterly of Applied Mathematics*, 26(2), 1968, 219-229.
- [35] Singhatanadgid, P., and Singhanart, T., The Kantorovich method applied to bending, buckling, vibration, and 3D stress analyses of plates: A literature review, *Mechanics of Advanced Materials and Structures*, 26(2), 2019, 170-188.
- [36] Shufrin, I., Rabinovitch, O., and Eisenberger, M., A semi-analytical approach for the geometrically nonlinear analysis of trapezoidal plates, *International Journal of Mechanical Sciences*, 52(12), 2010, 1588-1596.
- [37] Joodaky, A., Joodaky, I., Hedayati, M., Masoomi, R., and Farahani, E. B., Deflection and stress analysis of thin FGM skew plates on Winkler foundation with various boundary conditions using extended Kantorovich method, *Composites Part B: Engineering*, 51, 2013, 191-196.
- [38] Joodaky, A., and Joodaky, I., A semi-analytical study on static behavior of thin skew plates on Winkler and Pasternak foundations, *International Journal of Mechanical Sciences*, 100, 2015, 322-327.
- [39] Rajabi, J., and Mohammadimehr, M., Bending analysis of a micro sandwich skew plate using extended Kantorovich method based on Eshelby-Mori-Tanaka approach, *Computers and Concrete*, 23(5), 2019, 361-376.
- [40] Eisenberger, M., and Alexandrov, A., Buckling loads of variable thickness thin isotropic plates, *Thin-Walled Structures*, 41(9), 2003, 871-889.
- [41] Shufrin, I., and Eisenberger, M., Stability of variable thickness shear deformable plates—first order and high order analyses, *Thin-Walled Structures*, 43(2), 2005, 189-207.
- [42] Shufrin, I., Rabinovitch, O., and Eisenberger, M., Buckling of laminated plates with general boundary conditions under combined compression, tension, and shear—A semi-analytical solution, *Thin-Walled Structures*, 46(7-9), 2008, 925-938.
- [43] Eisenberger, M., and Shufrin, I., Buckling of plates by the multi term extended Kantorovich method, *7th EUROMECH Solid Mechanics Conference*, Lisbon, Portugal, 2009.
- [44] Jones, R. M., *Buckling of bars, plates, and shells*, Bull Ridge Corporation, 2006.
- [45] Eslami, M. R., Eslami, J., and Jacobs, *Buckling and postbuckling of beams, plates, and shells*, Springer, 2018.
- [46] Zhang, D.-G., and Zhou, Y.-H., A theoretical analysis of FGM thin plates based on physical neutral surface, *Computational Materials Science*, 44(2), 2008, 716-720.
- [47] Wang, X., and Yuan, Z., Buckling analysis of isotropic skew plates under general in-plane loads by the modified differential quadrature method, *Applied Mathematical Modelling*, 56, 2018, 83-95.
- [48] Khan, T., Zhang, N., and Akram, A. State of the art review of Functionally Graded Materials, *2019 2nd International Conference on Computing, Mathematics and Engineering Technologies (iCoMET)*, 2019, 30-31 Jan. 2019.
- [49] Ghannadpour, S., Ovesy, H., and Nassirnia, M., Buckling analysis of functionally graded plates under thermal loadings using the finite strip method, *Computers & Structures*, 108, 2012, 93-99.
- [50] Zhang, D.-G., Modeling and analysis of FGM rectangular plates based on physical neutral surface and high order shear deformation theory, *International Journal of Mechanical Sciences*, 68, 2013, 92-104.
- [51] Hassan Ahmed Hassan, A., and Kurgan, N., Modeling and Buckling Analysis of Rectangular Plates in ANSYS, *International Journal of Engineering & Applied Sciences*, 11(1), 2019, 310-329.
- [52] Yu, T., Yin, S., Bui, T. Q., Liu, C., and Wattanasakulpong, N., Buckling isogeometric analysis of functionally graded plates under combined thermal and mechanical loads, *Composite Structures*, 162, 2017, 54-69.
- [53] Kiani, Y., Bagherizadeh, E., and Eslami, M., Thermal buckling of clamped thin rectangular FGM plates resting on Pasternak elastic foundation (Three approximate analytical solutions), *ZAMM-Journal of Applied Mathematics and Mechanics/Zeitschrift für Angewandte Mathematik und Mechanik*, 91(7), 2011, 581-593.
- [54] Zhao, X., Lee, Y., and Liew, K. M., Mechanical and thermal buckling analysis of functionally graded plates, *Composite Structures*, 90(2), 2009, 161-171.

## ORCID iD

Ahmed Hassan Ahmed Hassan  <https://orcid.org/0000-0002-4880-0184>

Naci Kurgan  <https://orcid.org/0000-0001-7297-7249>

Nitat Can  <https://orcid.org/0000-0002-5741-0890>



© 2020 by the authors. Licensee SCU, Ahvaz, Iran. This article is an open access article distributed under the terms and conditions of the Creative Commons Attribution-NonCommercial 4.0 International (CC BY-NC 4.0 license) (<http://creativecommons.org/licenses/by-nc/4.0/>).

How to cite this article: Hassan A.H.A., Kurgan N., Can N. The Relations between the Various Critical Temperatures of Thin FGM Plates, *J. Appl. Comput. Mech.*, 6(SI), 2020, 1404-1419. <https://doi.org/10.22055/JACM.2020.34697.2459>

